Relativistic Runaway Ionization Fronts

A. Luque
Instituto de Astrofísica de Andalucía, IAA-CSIC, P.O. Box 3004, 18080 Granada, Spain
(Received 26 July 2013; published 29 January 2014)

We investigate the first example of self-consistent impact ionization fronts propagating at relativistic speeds and involving interacting, high-energy electrons. These fronts, which we name relativistic runaway ionization fronts, show remarkable features such as a bulk speed within less than one percent of the speed of light and the stochastic selection of high-energy electrons for further acceleration, which leads to a power-law distribution of particle energies. A simplified model explains this selection in terms of the overrun of Coulomb-scattered electrons. Appearing as the electromagnetic interaction between electrons saturates the exponential growth of a relativistic runaway electron avalanche, relativistic runaway ionization fronts may occur in conjunction with terrestrial gamma-ray flashes and thus explain recent observations of long, power-law tails in the terrestrial gamma-ray flash energy spectrum.

DOI: 10.1103/PhysRevLett.112.045003 PACS numbers: 52.80.Mg, 05.90.+m, 92.60.Pw

Introduction.—Relativistic runaway electron avalanches (RREAs) [1] are the keystone component of the nascent field of high-energy atmospheric physics [2]. A RREA consists of an exponentially growing number of relativistic electrons that, when accelerated by an external electric field, have overcome the stopping power of their medium (generally air) and are able to ionize further molecules. Since RREAs develop even below the conventional breakdown field for air, it has been suggested that they play a role in the inception of lightning [3] and that they may develop in the quasistatic fields above a charged thundercloud [4]. Although the evidence on these two issues is not conclusive, it is well established that RREAs play a central role in terrestrial gamma-ray flashes (TGFs). First observed in 1994 [5], TGFs are bursts of gamma rays emitted from electric storms lasting between some tens of microseconds and one millisecond. They were originally observed from the BATSE instrument aboard the Compton Gamma-ray Observatory spacecraft; later they have also been detected by the Reuven Ramaty High Energy Solar Spectroscopic Imager (RHESSI) [6,7], the aircraft-bounded ADELE [8,9], the Astrorivelatore Gamma a Immagini LEggero (AGILE) satellite [10–12] and, most recently, the Fermi spacecraft [13].

The main evidence that RREAs are the building block of TGFs comes from the coincidence of the energy spectrum of bremsstrahlung photons emitted from a RREA with the spectrum of photons captured by RHESSI [14–16]. However, the picture is complicated by two issues. First, the avalanche multiplication provided by realistic thundercloud fields is not enough to explain the high photon fluxes detected at satellite altitudes. Two mechanisms are viable explanations for the missing multiplication factor: relativistic feedback [17–19], whereby counterpropagating positrons and x-ray photons initiate many additional avalanches, and thermal runaway [20–23], which posits that many electrons are accelerated to high energies by the extreme electric fields in the streamer corona of lightning leaders. Recently, Tsuchiya *et al.* have measured the continuous emission of gamma radiation from a thundercloud that suddenly stops before a lightning stroke [24]. Although a direct connection with TGFs has not been established, this continuous radiation suggests that large-scale electric fields inside the cloud are sufficiently intense to accelerate electrons up to relativistic energies, thus lending support to the relativistic feedback model. Nevertheless, they do not necessarily rule out the thermal runaway process.

The second issue was raised when AGILE, sensitive to photon energies above the $\sim$10 MeV upper limit of RHESSI, measured a photon energy spectrum significantly harder (i.e., flatter) than the RREA spectrum [11], approaching a power law for energies up to about 100 MeV. The thermal runaway theory can fit this spectra [23] within the appropriate energy range, but does not predict a power law. Until now there has been no attempt to link the relativistic feedback theory with the AGILE observations. Note, however, that it has been recently suggested [13] that the high-energy AGILE spectra may result from a contamination by cosmic rays.

In this Letter, we investigate the fate of a RREA when its growth saturates due to the interaction between its constituent electrons. Although the electromagnetic interaction between particles in a RREA has received little attention [25], below we describe a plausible thundercloud scenario where this interaction becomes as relevant as the static field. After saturation, a RREA evolves into a front that we name relativistic runaway ionization front (RRIF). An outstanding property of RRIFs is that they act as efficient particle accelerators, filtering out low-energy particles. Having a spectrum of electron energies that approaches a power law for a significant range of energies, RRIFs are plausible candidates to explain the AGILE observations within the framework of relativistic feedback.

In a low-energy electric discharge, when the charge separation inside a growing electron avalanche is enough

to screen the background electric field, the avalanche develops into a streamer front. Afterwards, at lengths scales comparable to or smaller than the front width, the front dynamics is captured by a planar front model with small corrections due to a nonzero curvature [26–28]. This behavior is essentially preserved when the particles composing the avalanche propagate close to the speed of light; RRIFs are thus the high-energy counterpart to ionization fronts in low-energy electric discharges and here we start their study by treating them as planar fronts.

Focusing on planar fronts is especially justified by the stratified structure of thunderclouds. As we will see, the longitudinal extension of a RRIF is about 25 m at atmospheric pressure (Fig. 1), or about 100 m in a thundercloud. An electrified thundercloud, on the other hand, spans a few kilometers horizontally; an extensive discharge may therefore inject a population of electrons with a typical transversal length significantly longer than the characteristic front width. In the example that we shall work out later, these electrons have to propagate about 400 m for the emergence of a RRIF; in many cases this is still significantly shorter than the transversal length scale.

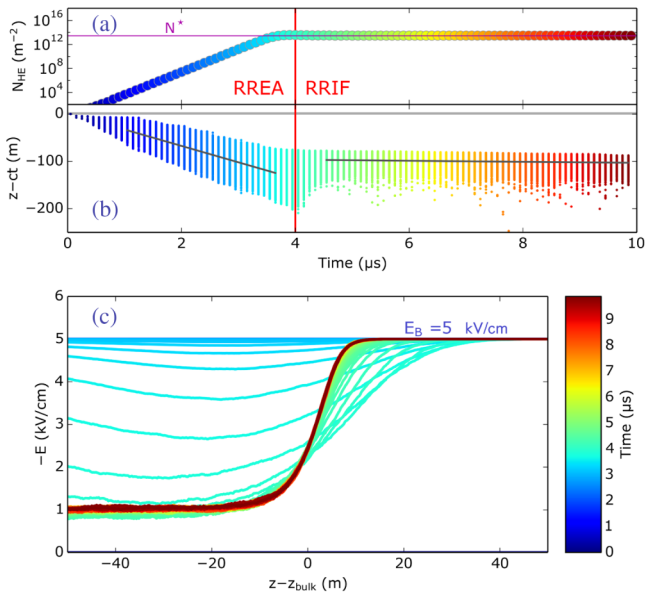

FIG. 1 (color online). Transition between a RREA and a RRIF under a background field $E_B = 5$ kV/cm. (a) After an phase of exponential growth, the number of high-energy electrons N_{HE} saturates when it screens the background field; the avalanche then transforms into a RRIF. (b) Location of electrons with energies above K_{th}. We plot $z - ct$ in order to emphasize small deviations from a propagation at the speed of light c. The straight segments represent linear fits for the location of all particles as functions of time for the corresponding intervals. They correspond to velocities of $0.88c$ in the RREA regime and $0.996c$ in the RRIF regime. The propagating front (c) screens the upstream electric field, although not completely. The colors in (c) represent different snapshots in time, as indicated by the color bar, and colors in panels (a) and (b).

Although we will focus on the possible generation of RRIFs by a horizontally extended discharge, it is possible that the electrons outgoing from a leader corona due to a thermal runaway also interact significantly and form an ionization front. Transversal diffusion in a RREA is faster than the longitudinal one [2] and electric-field screening acts also within a relativistic avalanche so, by analogy with low-energy discharges, it is likely that localized avalanches also evolve into fronts with the properties that we discuss below.

Model.—The physics of relativistic runaway is dominated by collisions between electrons and neutral gas molecules. The rates of all relevant processes are therefore proportional to the gas density n_{gas}, leading to well-known scaling laws [2]: typical lengths and times scale as $1/n_{\mathrm{gas}}$; electric fields and surface charge densities scale as n_{gas}. Here we shall follow the convention of expressing all magnitudes corresponding to air density at standard temperature and pressure, $n_{\mathrm{gas}}^{\mathrm{STP}}$. To translate our results to a different air density, electric fields have to be divided by a factor $\chi = n_{\mathrm{gas}}^{\mathrm{STP}}/n_{\mathrm{gas}}$, whereas times and lengths must be multiplied by χ. For example, in the Earth's atmosphere, at altitudes between 10 and 15 km, where TGFs are generated, χ ranges from 3 to 6.

We modeled the self-consistent dynamics of runaway electrons using a Monte Carlo, particle-in-cell code with one spatial dimension (z) and three momentum and velocity components ($p_{x,y,z}$, $v_{x,y,z}$). Here we sketch the main characteristics of the numerical model; further details are provided at the Supplemental Material [29].

The model follows individual electrons with high energy, i.e., kinetic energies above a predefined threshold $K_{\mathrm{th}} = 10$ keV. Low-energy electrons, also called thermal electrons, as well as positive ions, are considered immobile at the time scale of the model.

Each electron i accelerates due to the electrostatic force $-eE(z_i)$. The stopping power of air, F_D is due to ionizing collisions with air molecules and bremsstrahlung collisions with nuclei. The electrons ionize air molecules with an effective Møller cross section. As initially proposed by Lehtinen *et al.* [30], we only track individually ionization events where the kinetic energy of both out coming electrons is above K_{th}; the effect of the remaining collisions is accounted for by an effective friction force F_D^{ion} that acts opposite to the electron's momentum. For energies of some tens of MeV, bremsstrahlung becomes the dominant energy loss process, contributing an additional friction F_D^{bs} [31]. Finally, as proposed by Dwyer [32], we model elastic collisions with a shielded-Coulomb differential cross section.

In general, the complete Maxwell equations are required to compute the electromagnetic field generated by a ensemble of relativistic particles. However, this is considerably simplified by our assumption of planar symmetry. In this case, the Maxwell equations reduce to the one-dimensional (1D) Poisson equation $\varepsilon_0 \partial_z E = \rho(z)$, where E

is the z component of the electric field, ρ is the volumetric charge density, and ε_0 is the vacuum permittivity. Note that in one dimension the electrostatic Poisson equation is local, not leading to the instantaneous field propagation in three-dimensional electrostatics

Results.—We run a simulation with a background electric field $E_B = 5$ kV/cm starting with a surface density of 100 m^{-2} electrons with energy 0.5 MeV at $z = 0$. As Fig. 1 shows, the first stage of evolution is a standard RREA, with an exponential increase in the number of high-energy particles. The avalanche saturates once the density of high-energy electrons N_{HE} reaches $N^\star = \varepsilon_0 E_B/e \approx 3 \times 10^{13}$ m^{-2}.

At that point the avalanche transforms into a uniformly propagating RRIF. The transition is clear when we look at the location of all electrons with energies above $K_{\rm th}$. Panel (b) of Fig. 1 plots $z - ct$ for each of these particles as well as linear fits of the high-energy particle locations as functions of time for intervals in the RREA and RRIF regimes. These fits show that, whereas an avalanche propagates significantly slower than c (best fit is $0.88c$), a self-consistent front propagates within 1% of the speed of light ($0.996c$). Note also that around the RREA-RRIF transition the particles lagging farther from the front are thermalized.

Panel (c) shows the convergence of the local electric field towards the uniformly propagating front. To the left of the front (upstream) the electric field is around 1 kV/cm, below the critical field for relativistic runaway (2.18 kV/cm) [2]. Electrons on that region are quickly thermalized. The self-consistent front achieves a faster speed than the average speed of its constituent particles due to the release of new particles through impact ionization in its leading edge and the thermalization of lagging particles in the back side of the front.

We turn now to the energy spectrum of electrons in a RRIF. For RRIFs embedded in different background fields E_B, Fig. 2 shows the distribution function $f(K)$ of the kinetic energy K of all electrons with energies above 100 keV. For comparison, we also show the spectrum of a RREA.

Because of the exponential growth of the avalanche [2], the RREA spectrum exhibits an exponential cutoff at 7.3 MeV. Once the RREA is saturated, this cutoff disappears and the spectrum is characterized by (a) a higher, sharp cutoff imposed by bremsstrahlung stopping at energies $K_{\rm max}$ such that $eE_B = F_D(K_{\rm max}) \approx F_D^{bs}(K_{\rm max})$ and (b) for driving electric fields $E_B \gtrsim 10$ kV/cm, in the range (1–100) MeV the distribution function is approximated by a power law with exponent $\eta \approx -1$. Since this is the most salient property of RRIFs, it is worth examining it further with a simplified model. Further details are provided in the Supplemental Material [29].

Let us assume that all high-energy electrons travel with the front at a velocity close to c and are located at the

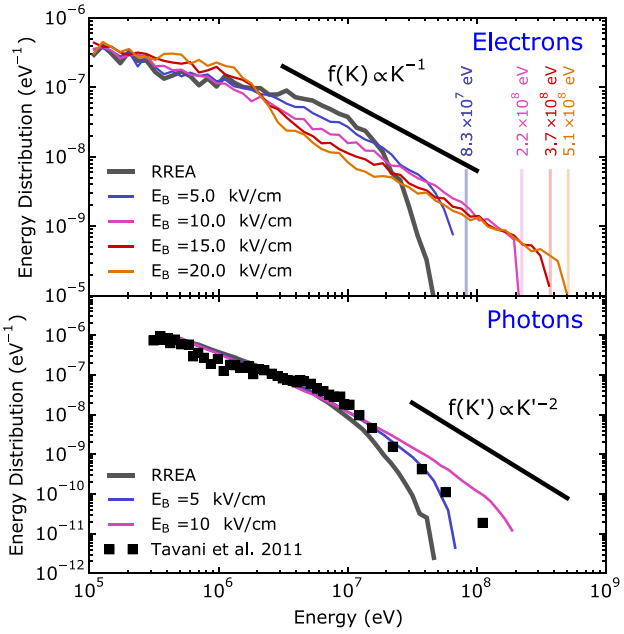

FIG. 2 (color online). Upper panel: Distribution function $f(K)$ of RRIF electron energies K with different background electric fields E_B. The vertical bars indicate the bremsstrahlung cutoff energy $K_{\rm max}$ (see text). We also show the slope of a power-law spectra with exponent $\eta = -1$ and the spectrum of a RREA under a uniform background electric field $E_B = 5$ kV/cm; the RREA spectrum depends weakly on the driving electric field. Lower panel: Distribution function $f(K')$ of energies K' of bremsstrahlung photons emitted from a RREA and a RRIF and an aggregate spectrum measured from AGILE [11].

midpoint where the electric field is $\sim -E_B/2$. For most of the relevant energies and for E_B above 10 kV/cm we can also assume that $eE_B/2 - F_D \approx eE_B/2$. Our simplified model considers that most of the time the electrons are traveling undisturbed in the forward direction but that, occasionally, they are elastically scattered by a nucleus; if the scattering angle θ is larger than some threshold $\theta_{\rm th}$, the electrons are overrun by the front and they are thermalized upstream, otherwise they recover their forward propagation. Integrating the electron's equations of movement we find [29] that after a scattering with angle $\theta \ll 1$, the total distance lost by the electron relative to the front is, to leading order, $cp\theta^2/eE_B$, where p is the electron's momentum. By setting this distance to half the front width ℓ, we arrive at the threshold angle

$$\theta_{\rm th}^2 = \frac{eE_B\ell}{2cp}. \tag{1}$$

Integrating the elastic scattering cross section we obtain the rate ν of collisions with $\theta > \theta_{\rm th}$,

$$\nu = \frac{M}{eE_B \ell K}, \tag{2}$$

where $M = 16\pi n_{\rm gas} Z^2 r_e^2 m^2 c^5$ (Z: average atomic number of air nuclei, r_e: classical electron radius, m: electron mass).

Since newly liberated electrons start with an energy far below the energies of interest (1–100) MeV, the evolution of the distribution function in this range is described by

$$\frac{\partial f}{\partial t} = -\frac{ceE_B}{2}\frac{\partial f}{\partial K} - \nu(K) f = 0, \tag{3}$$

where the last equality holds in a steady-state front.

In a uniformly propagating front, the total energy of the high-energy electrons is time independent. Together with Eqs. (2) and (3), this leads to $\ell = 2M/ce^2E_B^2$ and $\partial f/\partial K + f/K = 0$, solved by $f \propto K^{-1}$. We emphasize that the key ingredient for the power law with exponent $\eta = -1$ is $\nu \propto K^{-1}$; i.e., the average time $\tau = 1/\nu$ that an electron spends in the high-field side of the front is proportional to its energy. Thus, the front stochastically filters out electrons with low energy or with a slanted direction, favoring a population of high-energy, strongly beamed electrons.

The lower panel of Fig. 2 shows the energy spectrum of bremsstrahlung photons emitted from a RRIF. We also plot the spectrum of a RREA and the aggregate spectrum measured from the AGILE spacecraft [11]. Since the cross section for an electron with energy K to emit a bremsstrahlung photon with energy $K' < K$ is roughly proportional to $1/K'$, the electron distribution $f(K) \propto K^{-1}$ leads to a photon spectrum $f(K') \propto K'^{-2}$. This is harder than the power-law exponent 2.7 ± 0.1 reported by Tavani *et al.* [11] but the difference may be explained by the contribution of lower driving electric fields (e.g., $E_B = 5$ kV/cm), with softer spectra.

Discussion.—Here we have investigated the interaction between relativistic runaway electrons by first reducing the problem to one dimension. A self-consistent 2D model of RRIFs is presently unfeasible due to the large number of superparticles required to describe the complete front. However, we can check that the 1D model provides reliable results by comparing with the fields in a non-self-consistent 2D simulation as follows. First we included the transversal (x, y) dynamics of particles inside our Monte Carlo model. We run a simulation initialized by a bunch of electrons at a single point in the z axis with equal velocities pointing in the z direction. Then we introduced the current density resulting from this simulation into a cylindrically symmetric finite-differences time-domain electromagnetic solver [33]. The resulting electric field within the avalanche region exhibits the same screening features as the solution of the 1D Poisson equation and is accurately approximated by it.

These results indicate that RRIFs are the generic saturation mechanism of a RREA, so given enough space all RREAs will evolve into RRIF-like fronts. However, two issues deserve to be discussed further: (a) whether RRIFs are likely to emerge from realistic thundercloud fields and (b) whether they explain the hard TGF spectra observed from AGILE.

Regarding (a), we propose the following scenario based on the theory of relativistic feedback [17,19]. We consider a vertically stratified field distribution composed by a high-field region that undergoes a relativistic feedback discharge and feeds high-energy electrons into a region with a lower field. For concreteness, say that the initial fields are, respectively, $E_B^{\rm high} = 10$ kV/cm and $E_B^{\rm low} = 5$ kV/cm. According to [32] the discharge times are about $\tau^{\rm high} = 10\ \mu$s and $\tau^{\rm low} = 20\ \mu$s. The feedback discharge in the high-field region produces a peak flux $F \approx 10^{19}$ m^{-2} s^{-1} of high-energy electrons [32] that enters into the low field region. In a slice of about $\ell = 30$ m, which is the width of the RRIF in Fig. 1, the flux translates into a density $\sim F\ell/c = 10^{12}$ m$^{-2} \approx N^\star/30$ of high-energy electrons. Hence the low-field region has to provide only a multiplication factor 30 to reach a RRIF regime. Since $\tau^{\rm low} < \tau^{\rm high}$ the low-field region has not yet discharged and it is able to provide that multiplication factor within a distance $\sim \lambda \log(30) \approx 100$ m, where $\lambda \approx 30$ m is the avalanche multiplication length at $E_B^{\rm low}$ [29]. Remember that these numbers refer to air at standard temperature and pressure; the required width of the low field region scales to about 400 m at thundercloud altitudes. Note also that in this example the electron energy spectrum of the RRIF would extend up to about 80 MeV, corresponding to the bremsstrahlung cutoff for $E_B = 5$ kV/cm (see Fig. 2).

The previous estimations suggest that RRIFs may plausibly occur spontaneously in thundercloud fields. This is also supported by the power-law tail in the distribution of TGF intensities at their source [34], which suggests that there may exist TGFs intense enough to reach the RRIF regime. RRIFs may be also triggered by strong extensive air showers generated by energetic cosmic rays impinging into a thundercloud. We also speculate that they are likely in giant planets with strong electrical activity, such as Jupiter and Saturn [35], where there is more space for large avalanche multiplication.

We now address the second issue (b) mentioned above: whether RRIFs have already been spotted in the hard spectra measured by AGILE [11]. Despite the resemblance of the spectra in Fig. 2, the evidence is not conclusive and the AGILE data have yet to be confirmed independently by another mission to rule out the possibility of cosmic ray contamination. Note that an RRIF scenario would naturally explain the existence of two TGF populations, a low-energy one characterized by a RREA spectrum and a high-energy, RRIF one with a power-law spectrum. Typical TGF time scales, extending up to one millisecond, are too long for a single RRIF so if RRIFs are responsible for a significant component of TGF emissions, they likely appear as a series of bursts as a large thundercloud region discharges nonuniformly.

The analogy with low-energy discharge physics suggests that RRIF fronts will likely appear as localized, streamer-like [27] curved discharges. In that case a subset of high-energy electrons may accelerate to energies exceeding the total electrostatic potential available in the thundercloud by surfing the enhanced field ahead of a curved front. This phenomenon would explain electron energies above 100 MeV in a TGF. More detailed observations of the high-energy tail of TGF spectra as well as improved models are required to investigate this possibility.

From a broader point of view, the theoretical relevance of RRIFs stems from their ability to self-organize into a configuration where a proportionally larger fraction of the electric-field energy is transferred into the already most energetic particles. They are spontaneously generated, efficient particle accelerators.

We acknowledge support from Spanish MINECO under project AYA2011-29936-C05-02 and by the Junta de Andalucia, Proyecto de Excelencia FQM-5965.

[1] A. V. Gurevich, G. M. Milikh, and R. Roussel-Dupre, Phys. Lett. A **165**, 463 (1992).
[2] J. R. Dwyer, D. M. Smith, and S. A. Cummer, Space Sci. Rev. **173**, 133 (2012).
[3] A. V. Gurevich and A. N. Karashtin, Phys. Rev. Lett. **110**, 185005 (2013).
[4] M. Füllekrug, R. Roussel-Dupré, E. M. D. Symbalisty, J. J. Colman, O. Chanrion, S. Soula, O. van der Velde, A. Odzimek, A. J. Bennett, V. P. Pasko *et al.*, Atmos. Chem. Phys. **11**, 7747 (2011).
[5] G. J. Fishman, P. N. Bhat, R. Mallozzi, J. M. Horack, T. Koshut, C. Kouveliotou, G. N. Pendleton, C. A. Meegan, R. B. Wilson, W. S. Paciesas *et al.*, Science **264**, 1313 (1994).
[6] B. W. Grefenstette, D. M. Smith, B. J. Hazelton, and L. I. Lopez, J. Geophys. Res.: Space Phys. **114**, A02314 (2009).
[7] T. Gjesteland, N. Østgaard, A. B. Collier, B. E. Carlson, C. Eyles, and D. M. Smith, Geophys. Res. Lett. **39**, L05102 (2012).
[8] D. M. Smith, J. R. Dwyer, B. J. Hazelton, B. W. Grefenstette, G. F. M. Martinez-McKinney, Z. Y. Zhang, A. W. Lowell, N. A. Kelley, M. E. Splitt, S. M. Lazarus *et al.*, J. Geophys. Res.: Atmos. **116**, D20124 (2011).
[9] D. M. Smith, J. R. Dwyer, B. J. Hazelton, B. W. Grefenstette, G. F. M. Martinez-McKinney, Z. Y. Zhang, A. W. Lowell, N. A. Kelley, M. E. Splitt, S. M. Lazarus *et al.*, Geophys. Res. Lett. **38**, L08807 (2011).
[10] M. Marisaldi, A. Argan, A. Trois, A. Giuliani, M. Tavani, C. Labanti, F. Fuschino, A. Bulgarelli, F. Longo, G. Barbiellini *et al.*, Phys. Rev. Lett. **105**, 128501 (2010).
[11] M. Tavani, M. Marisaldi, C. Labanti, F. Fuschino, A. Argan, A. Trois, P. Giommi, S. Colafrancesco, C. Pittori, F. Palma *et al.*, Phys. Rev. Lett. **106**, 018501 (2011).
[12] F. Fuschino, M. Marisaldi, C. Labanti, G. Barbiellini, E. Del Monte, A. Bulgarelli, M. Trifoglio, F. Gianotti, M. Galli, A. Argan *et al.*, Geophys. Res. Lett. **38**, L14806 (2011).
[13] M. S. Briggs, S. Xiong, V. Connaughton, D. Tierney, G. Fitzpatrick, S. Foley, J. E. Grove, A. Chekhtman, M. Gibby, G. J. Fishman *et al.*, J. Geophys. Res.: Space Phys. **118**, 3805 (2013).
[14] J. R. Dwyer and D M. Smith, Geophys. Res. Lett. **32**, L22804 (2005).
[15] B. E. Carlson, N. G. Lehtinen, and U. S. Inan, Geophys. Res. Lett. **34**, L08809 (2007).
[16] N. Østgaard, T. Gjesteland, J. Stadsnes, P. H. Connell, and B. Carlson, J. Geophys. Res. **113**, A02307 (2008).
[17] L. P. Babich, E. N. Donskoy, I. M. Kutsyk, and R. A. Roussel-Dupré, Geophys. Res. Lett. **32**, L09809 (2005).
[18] J. R. Dwyer, J. Geophys. Res. **113**, D10103 (2008).
[19] J. R. Dwyer, J. Geophys. Res. **117**, A02308 (2012).
[20] G. D. Moss, V. P. Pasko, N. Liu, and G. Veronis, J. Geophys. Res. **111**, A02307 (2006).
[21] C. Li, U. Ebert, and W. Hundsdorfer, J. Phys. D **42**, 202003 (2009).
[22] O. Chanrion and T. Neubert, J. Geophys. Res.: Space Phys. **115**, A00E32 (2010).
[23] S. Celestin, W. Xu, and V. P. Pasko, J. Geophys. Res. **117**, A05315 (2012).
[24] H. Tsuchiya, T. Enoto, K. Iwata, S. Yamada, T. Yuasa, T. Kitaguchi, M. Kawaharada, K. Nakazawa, M. Kokubun, H. Kato *et al.*, Phys. Rev. Lett. **111**, 015001 (2013).
[25] A. V. Gurevich, K. P. Zybin, and Y. V. Medvedev, Phys. Lett. A **349**, 331 (2006).
[26] U. Ebert and W. van Saarloos, Physica D (Amsterdam) **146D**, 1 (2000).
[27] U. Ebert, F. Brau, G. Derks, W. Hundsdorfer, C.-Y. Kao, C. Li, A. Luque, B. Meulenbroek, S. Nijdam, V. Ratushnaya *et al.*, Nonlinearity **24**, C1 (2011).
[28] A. Luque and F. J. Gordillo-Vázquez, Nat. Geosci. **5**, 22 (2012).
[29] See Supplemental Material at http://link.aps.org/supplemental/10.1103/PhysRevLett.112.045003 for more details on our numerical model as well as the sketch of an analytical model of RRIFs, including derivations of Eqs. (1) and (2).
[30] N. G. Lehtinen, T. F. Bell, and U. S. Inan, J. Geophys. Res. **104**, 24699 (1999).
[31] M. J. Berger, J. S. Coursey, M. A. Zucker, and J. Chang, Stopping-Power and Range Tables for Electrons, Protons, and Helium Oons, http://www.nist.gov/pml/data/star/index.cfm.
[32] J. R. Dwyer, Phys. Plasmas **14**, 042901 (2007).
[33] U. Inan and R. Marshall, *Numerical Electromagnetics: The FDTD Method* (Cambridge University Press, Cambridge, 2011).
[34] A. B. Collier, T. Gjesteland, and N. Østgaard, J. Geophys. Res. **116**, A10320 (2011).
[35] Y. Yair, Adv. Space Res. **50**, 293 (2012).